Check for updates

SOCIAL SCIENCES

Wealth and land-cover change govern landslide fatalities on world's mountains

Seçkin Fidan[1,2]*, Tolga Görüm[2], Abdullah Akbaş[3], Bikem Ekberzade[2], Ugur Ozturk[4,5]

Copyright © 2026 The Authors, some rights reserved; exclusive licensee American Association for the Advancement of Science. No claim to original U.S. Government Works. Distributed under a Creative Commons Attribution NonCommercial License 4.0 (CC BY-NC).

Despite the common perception, most fatal landslides occur in human-transformed environments. Even on steep terrain, anthropogenic disturbances may fundamentally modulate landslides. Most of our knowledge regarding landslide-human interaction is restricted to local models or regional heuristic assessments based on empirical evidence. In this study, we used land-use–land-cover change as a metric to explain human pressure as a preconditioning factor for fatal landslide occurrences to provide a global overview. We addressed countries' income levels, populations, exposure, and a dataset of ≈60 years of land-use–land-cover changes with mountainous landmasses to compare landslides and fatalities across 46 countries. Our statistical analyses show that land-use–land-cover changes have a substantially greater influence on the density of fatal landslides and landslide fatalities than physical factors such as topography and precipitation, especially in lower-income countries. We observed a marginal landslide impact when the land-use–land-cover change was low, regardless of the income class. Our results emphasize that effective land-use–land-cover planning is critical to decreasing landslide fatalities, especially in low- and lower-middle–income countries.

INTRODUCTION

Among the most destructive hazards, landslides typically kill more than 4500 people (2004 to 2019) (*1*) and cause US$20 billion in damage annually (<2014) (*2*). In 2024, for instance, 766 fatal landslides claimed 4933 lives, indicating an unprecedented year of fatal landslide occurrences, as the count has been under 500 since 2004 (*3*). These substantial counts of fatal landslides are distributed unevenly among nations. We aim to answer why landslides are deadlier in certain regions than others with comparable potential concerning topographic relief and climate. Beyond national wealth, climate, population density, and hazard awareness, we propose that increasing human pressure on fragile mountainscapes, depicted as land-use–land-cover change (LULCC), is a key aspect modulating landslide fatalities (*4*–*7*).

Besides being exposed, human alterations to the land surface may also alter landslide occurrences (*8*). Approximately 60% of the mountainous areas are under intense human pressure (*9*). The number of people exposed to natural hazards in mountain areas doubled between 1975 and 2015 (*10*, *11*), quicker than the average population rise (*12*). Clear-cutting and the transition of forests to pasture and cropland alter hillslope hydrology, decreasing slope stability (*13*–*15*). Activities linked to mining infrastructures and road constructions disrupt the natural continuity of hillsides, destabilizing hillslopes (*16*–*18*). As a result, although the mean annual population exposed to landslides is expected to rise by about 90%, mean annual fatalities are projected to increase by 140% by 2060 (*19*).

We need a global understanding of how human pressure, measured as LULCC rate, influences landslides across mountain ranges. State-of-the-art research has explored the importance of increasing human pressure regionally (*20*, *21*), such as in the Andes (*4*, *22*), the Apennines (*6*), and the Kivu Rift (*23*), demonstrating a considerable role of LULCC on fatal landslide events and their fatalities. A global evaluation of landslide and land-use–land-cover interactions is complicated, as terrain conditions, land management strategies, population densities, and intercountry socioeconomic conditions vary considerably among mountainous communities. Until recently, we also lacked high-resolution global datasets, such as historic (>50 years) land-use–land-cover (*24*) and population data (*25*), which would allow exploring the above-listed differences. A lack of complete global landslide database also hinders such an assessment; however, there are efforts to track landslide fatalities globally to provide a rough proxy in this regard, thanks to community efforts (*1*).

To address these gaps, we adopted a K1 mountain characterization (*26*) and focused on mountainous areas of 46 countries (Fig. 1, A to D), categorized by income level. Initially, we calculated a ≈60-year-long land-use–land-cover (*24*) and a 45-year-long population (*25*) change rate and analyzed how these variables relate to landslide fatalities. We introduced a new metric, total LULCC rate (LC_{SN}), to quantify the overall change across multiple land-use–land-cover types. We also included population density, exposure, topographic relief, precipitation, and income level factors in our models. Thanks to the recent data advancements and this metric, we could build a statistical model to determine whether LULCC and population growth were associated with observed landslides and fatalities in mountainous areas.

In this study, we show that high-income (7%) and upper-middle–income (13%) countries show more stable and limited transitions in terms of LULCC. The change in mountainous areas of lower-middle–income (18%) and low-income (50%) countries is more pronounced. In addition, the increasing LULCC rate (LC_{SN}) correlates with a corresponding increase in the density of fatal landslides and the density of landslide fatalities in low- and lower-middle–income countries. For example, in some countries, such as Haiti, Sri Lanka, and El Salvador, the LULCC rate is directly associated with increased fatal landslides and the number of fatalities. However, the correlation weakens in high-income countries such as Switzerland, Japan, Italy, Austria, and South Korea despite favorable conditions for landslide occurrence considering topographic relief and climate.

[1]Department of Architecture and Urban Planning, Ankara University, Ankara 06100, Türkiye. [2]Eurasia Institute of Earth Sciences, Istanbul Technical University, Istanbul 34469, Türkiye. [3]Department of Geography, Faculty of Arts and Science, Bursa Uludag University, Bursa 16059, Türkiye. [4]Department of Geography and Regional Research, University of Vienna, Vienna 1010, Austria. [5]Section of Seismic Hazard and Risk Dynamics, GFZ Helmholtz Centre for Geosciences, Potsdam, 14473, Germany.
*Corresponding author. Email: seckinfidan@ankara.edu.tr

Downloaded from https://www.science.org on April 08, 2026

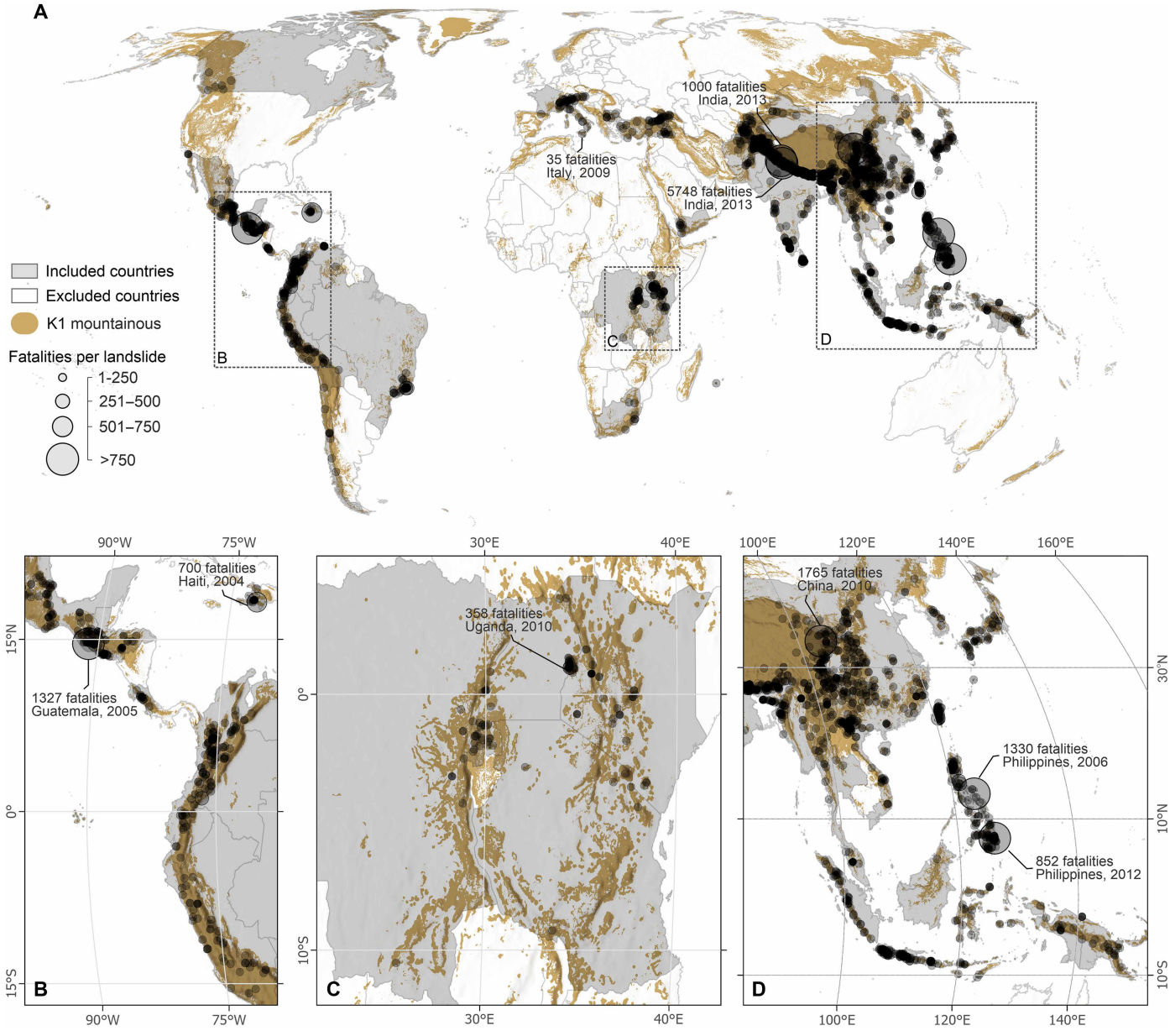

Fig. 1. Global distribution of fatal landslides in K1 mountainous areas. Panel (**A**) illustrates the distribution of fatal landslides in the K1 mountainous areas of countries. The K1 layer defines mountainous terrain based on a combination of elevation, hillslope angle, and topographic relief at a 1-km resolution. Panels (**B**) to (**D**) show close-up views of fatal landslides in Central America and the northern Andes, East Africa, and Southeast Asia, respectively. Gray shading highlights those countries with a minimum of six fatal landslides. The size of the landslide point represents the number of fatalities for each event.

We claim the differences in LULCC are among the main drivers behind the notable disparities in landslide impacts across national income levels. Although struck by major landslides frequently, the countries with low LULCC are also those least impacted in terms of fatalities, regardless of national wealth. For example, while Nepal is well known for landslide hazards, there are fewer landslide fatalities and lower LULCC rates below the average of the low-income category. Despite being recognized for landslide impacts, Colombia (*27*, *28*) also experiences lower fatalities with low LULCC in the lower-middle–income category. Hence, land-use–land-cover transitions appear to be a critical factor in explaining landslide fatalities aside from wealth.

RESULTS

Globally steady LULCCs

Overall, global land-use–land-cover—forest, grass and shrubland, pasture, sparse/no vegetation, cropland, and urban (given in the order of most to least favored in terms of landslide susceptibility)—in mountainous areas reveals relatively modest changes between 1960 and 2019. However, urban areas have doubled (fig. S1, A and B), and 4.5% of the sparse/no vegetation areas were converted to pasture. These two land-use–land-cover types represent most of the changes observed during this period (fig. S1C). Global land-use–land-cover dynamics show substantial differences when national wealth is considered (fig. S6).

Downloaded from https://www.science.org on April 08, 2026

Land-use–land-cover in high- and upper-middle–income countries has remained almost unchanged since 1960, with negligible transitions between land-use–land-cover categories in world's mountains (Fig. 2, A and B). LULCC was also small in lower-middle–income countries. The only notable change in this income category was a 9% transition from sparse/no vegetation to pasture (Fig. 2C). In contrast, the total transition between categories was around 50% in low-income countries (Fig. 2D). The data suggest that while only 7% of forest and 7% of pasture were transformed into a category that may be more landslide prone in the low-income group, when looked in detail, 17% of pasture was transformed into cropland, and more than 14% of forest was converted to pasture, grass, and shrubland. In addition, 7% of the grass and shrubland was transformed into forest cover. To account for such complex cross-transitions, we introduced an LULCC score (LC_S) metric to evaluate the overall anthropogenic impacts (see Materials and Methods).

Cross-country variation of LULCC

Recognizing the residual difference between countries and the average changes in their respective income categories, we explored LULCC at the country level across 46 countries individually (figs. S2 to S5 and tables S1 and S2). Some countries experienced changes that were

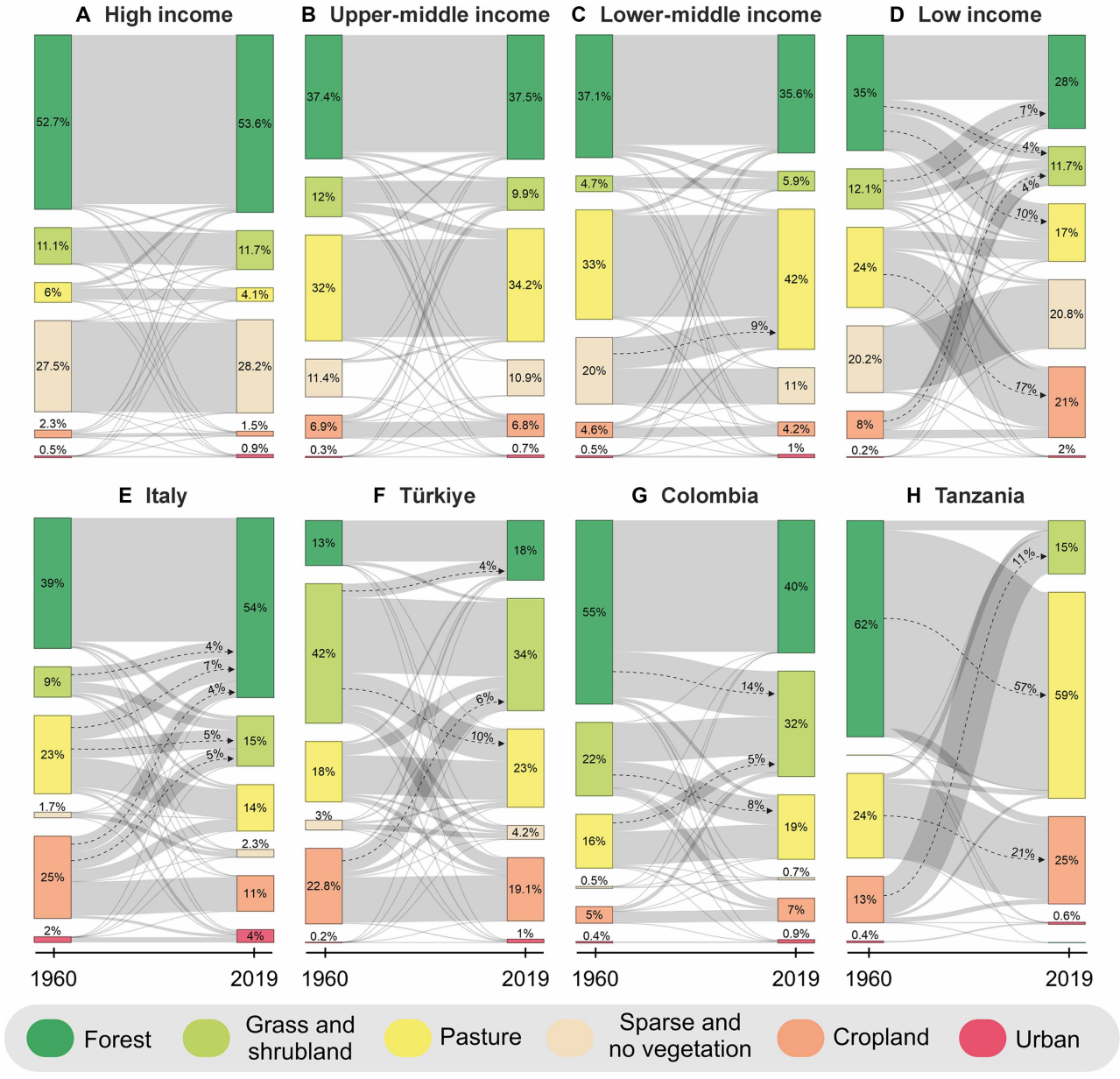

Fig. 2. Land-use–land-cover type transitions in mountainous areas by income classification between 1960 and 2019. Each bar represents the proportion (%) of different land-use–land-cover types, with each year summing to 100%. The gray color of the transitions indicates whether the land-use–land-cover type changes to the same or another type. The dashed arrow also indicates large transitions. Changes are ordered from up to down as most (i.e., forest) to least (i.e., urban) favored regarding landslide susceptibility.

Downloaded from https://www.science.org on April 08, 2026

well above average in their wealth category. For example, high- and upper-middle–income countries (figs. S2 and S3, respectively) were mainly stable, but there were some winners. For instance, Italy (Fig. 2E), Türkiye (Fig. 2F), and France (fig. S2) increased their forest cover by 15, 5, and 15%, respectively, in their mountainous terrain. However, the total anthropogenically induced LULCC score (LC_S) was 21% in Italy, 11% in France, and 32% in Türkiye, reflecting broader changes beyond sole forest gain (excluding forest; see LC_S values in Materials and Methods and table S1).

Lower- and middle-income countries remained generally stable, with some notable exceptions. For example, about 14% of Colombia's mountain forest cover had been lost to grass and shrubland (Fig. 2G), with the total LULCC in Colombia reaching 34% (table S2). On the contrary, Tanzania had lost its entire forest cover over country's mountains in the low-income category, with an LULCC score (LC_S) of 97% (Fig. 2H and table S2).

Although lower-middle–income countries showed relatively lower land-use–land-cover transformations, similar to wealthier nations, some in this group were ranked similar to low-income countries (see LC_S values in table S2). For instance, Ecuador, El Salvador, Guatemala, Indonesia, and Sri Lanka suffered losses of up to 20% of their forest cover, as did Colombia (fig. S4).

Because the range of mountainous regions between countries may differ compared to their actual size, we introduced a total LULCC rate (LC_{SN}) metric that normalizes the LULCC score (LC_S) to countries' landmass to allow intercountry comparisons (see Materials and Methods). Crucially, all variables were spatially masked to only consider the K1 mountainous areas before these calculations. For example, Rwanda lost nearly its entire forest cover in its mountainous area, which originally accounted for about 23% of the country's mountains. In contrast, India increased its forest cover by about 12%, more than Rwanda's entire mountain area (fig. S5 and table S2).

Controlling factors and model relationships

LULCC is a product of population growth (Fig. 3, A and B). Most countries in our subset (41 of 46) have experienced considerable population growth since 1960 (fig. S7). Wealthier countries, such as Japan, remained relatively steady. In contrast, economically disadvantaged nations exhibited about 2.5-fold higher population change when normalized with the country's mountain area (fig. S8).

To ensure comparability across nations, we aggregated landslide and fatality information within the mountainous area (K1) of each country. We calculated the density of fatal landslides (*LD*) and the density of landslide fatalities (*FD*) by dividing the total number of fatal events and deaths by the mountainous area of that country. This normalization provides a consistent measure of how concentrated fatal landslides and fatalities are across different mountainous terrains, accounting for variations in country size and mountainous extent. As the LULCC rate (LC_{SN}) increases, both density of fatal landslides (*LD*) and density of landslide fatalities (*FD*) show an increase (Fig. 3, C and E). Similarly, the population change rate (PC_N) also raises the density of landslides (*LD*) and fatalities (*FD*) (figs. S11B and S13B). These correlations are particularly pronounced in low- and lower-middle–income countries (Fig. 3, D and F, and figs. S11C and S13C). Overall, in countries with high anthropogenic pressures, the density of landslides and fatalities is typically higher (e.g., Haiti and Rwanda). However, the density of landslides (*LD*) and fatalities (*FD*) is limited in countries with low rates of population and LULCC (e.g., Canada).

Beyond these, we fitted the log-Gaussian generalized additive model (GAM), including population density (*PD*), exposure (*E*; see Materials and Methods), topographic relief, mean annual precipitation, and income level factors besides land-use–land-cover and population change rates. Before analyzing the relationships between the log-scale density of landslides (*LD*) and fatalities (*FD*) (fig. S14) and controlling factors, multicollinearity analysis was performed among the parameters (fig. S15). As a result, the factors of LULCC rate (LC_{SN}) with population change rate (PC_N) and population density (*PD*) report strong correlations [correlation coefficient (*r*): 0.88 and *r*: 0.87, respectively]. Therefore, of these three control factors, we only included LULCC rate (LC_{SN}) in the model and fitted GAM-LCC as the primary model (fig. S16).

On the basis of the GAM-LCC model, LULCC rate (LC_{SN}) is the variable with the highest positive effect on both the density of fatal landslides (*LD*) and the density of landslide fatalities (*FD*) (Fig. 4). As the LULCC rate (LC_{SN}), the positive effect increases in both models (Fig. 4A). Topographic relief and mean annual precipitation show positive effects, yet these effects are lower compared to human pressure. For the density of fatal landslides (*LD*), topographic relief is a positive effect above ≈700 m, while for the density of landslide fatalities (*FD*), its effect is limited and near zero (Fig. 4B). Mean annual precipitation has a positive effect after ≈1000 mm in both models (Fig. 4C).

Income group shows a stark difference in both the density of fatal landslides (*LD*) and the density of landslide fatalities (*FD*) models. Low- and lower-middle–income countries show the highest and most positive effect, while high- and upper-middle–income countries have a negative effect (Fig. 4D).

Land-cover transitions also seem particularly detrimental when investigated in the same income class. For instance, Nepal, a well-known landslide-prone country, has an LULCC rate (LC_{SN}) of only 0.08, leading to approximately four fatalities per landslide. In contrast, Rwanda, where the LULCC rate (LC_{SN}) is 0.9—more than 10 times higher than Nepal—experiences an average of more than seven fatalities per landslide (table S5). Similarly, in the high-income category, Switzerland, with an LULCC rate (LC_{SN}) nearly four times higher than France's, experiences a density of fatal landslides (*LD*) and a density of landslide fatalities (*FD*) over four times and seven times higher than France's (table S4). Consistent with our overall methodology, the comparison between France and Switzerland, so as between Rwanda and Nepal, is based specifically on their respective mountainous areas.

Alternatively, to minimize the strong multicollinearity between LULCC rate (LC_{SN}), population change rate (PC_N), and population density (*PD*), we used principal components analysis (PCA) to obtain a composite indicator representing human pressure (fig. S16). Then, the first principal component (PC1), explaining nearly 90% of the total variance, was extracted and used as a human pressure factor (table S3). Evaluating this model (GAM-PC1), we found the outputs to be indifferent (Fig. 4).

Model performance

To assess the consistency and robustness of the models, two different models were compared, including LULCC rate as a single proxy (GAM-LCC) and variables representing human pressures as a composite indicator (GAM-PC1). The observed and predicted values show strong agreement in both density of fatal landslides (*LD*) and density of landslide fatalities (*FD*) models (figs. S21A and

Downloaded from https://www.science.org on April 08, 2026

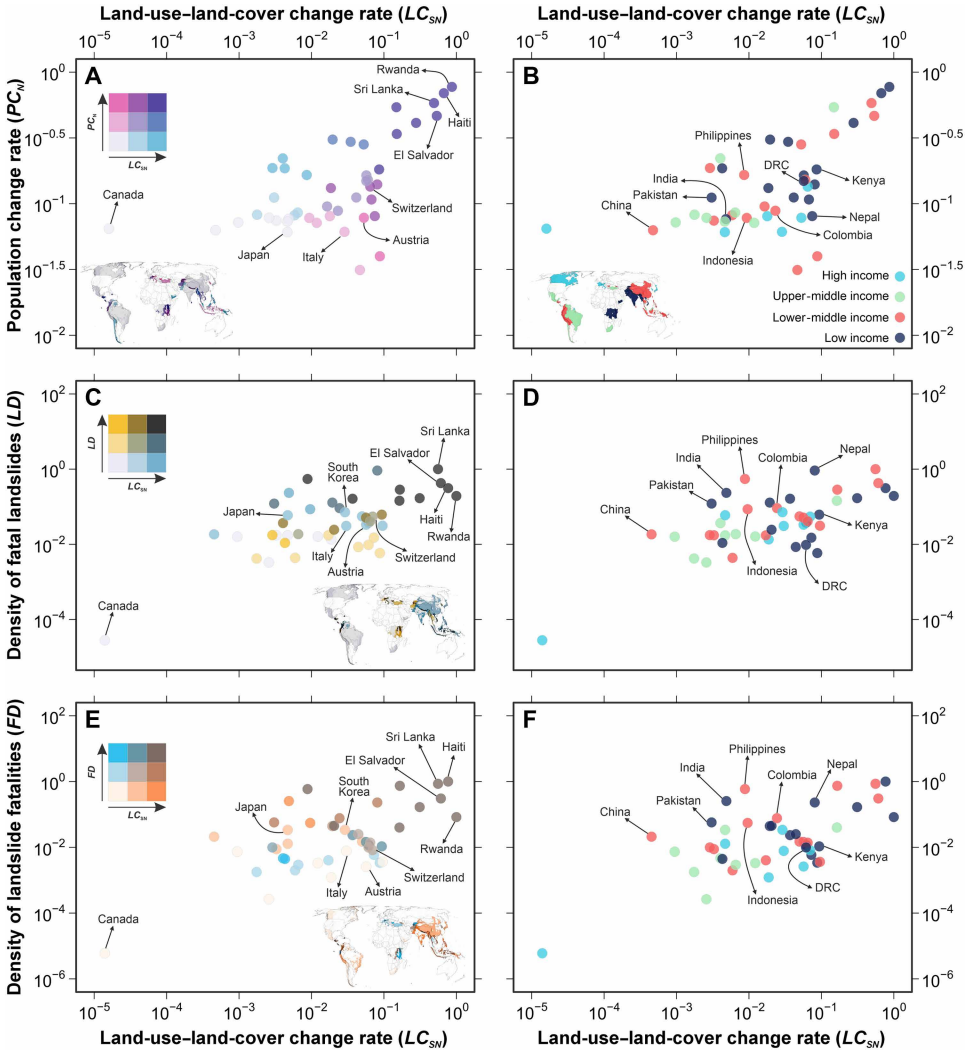

Fig. 3. Relationship between LULCC rate (LC_{SN}) and metrics of population change rate, density of fatal landslides, and density of landslide fatalities across countries. Subplots (**A**), (**C**), and (**E**) show the countries' LULCC rate (LC_{SN}) plotted against the population change rate (PC_N), density of fatal landslides (LD), and density of landslide fatalities (FD) as the bivariate combined distribution, respectively. Subplots (**B**), (**D**), and (**F**) show the same, but countries are categorized by wealth.

S22A, respectively). We observe that the quantile-quantile (QQ) plots, which are close to a straight line, show that the residuals largely agree with the theoretical distribution. At the same time, the histograms are consistent with normality and show good-fitting performance (figs. S21, B and C, and S22, B and C).

In general, both models perform well. GAM-PC1 (multiple variables representing human pressures) shows a slight superiority over GAM-LCC (single proxy of LULCC rate). We obtained slightly lower errors, higher correlations, and lower Akaike information criterion (AIC) values for both the density of fatal landslides (*LD*) and the density of landslide fatalities (*FD*). However, we emphasize that this difference is relatively minor, and models perform comparably good (full metrics are provided in table S6).

DISCUSSION

The major problem of globally increasing, in the best case, stagnating, landslide fatalities (*3*) is the continuously rising human pressure in mountainous regions (*7*, *12*). Addressing this problem requires assessments from environmental and socioeconomic perspectives. However, first, the source and scale of the issue need to be determined globally. Our primary contribution toward this goal is a global assessment of landslide incidence and fatalities compared to human-landscape interaction depicted as the rate of LULCC (e.g., soil sealing impact) (*20*).

The additional stress of anthropogenic climate change (*29*), increasing landslide susceptibility (*30*, *31*) of mountainous areas due to abrupt changes in climatic drivers, and the limited adaptive capacities of at-risk populations add to the challenges (*32*). Not only are the direct effects of human activities, such as deforestation, decisive, but also their indirect effects through land-use–land-cover, such as changes in soil and/or slope properties as a result of agricultural expansion and urban sprawl, need to be considered as potential preconditions or triggers of landslides in mountainous environments [e.g., (*33*)].

A decrease in income levels coupled with an increase in population rates often becomes a precursor to higher LULCC. We show

Downloaded from https://www.science.org on April 08, 2026

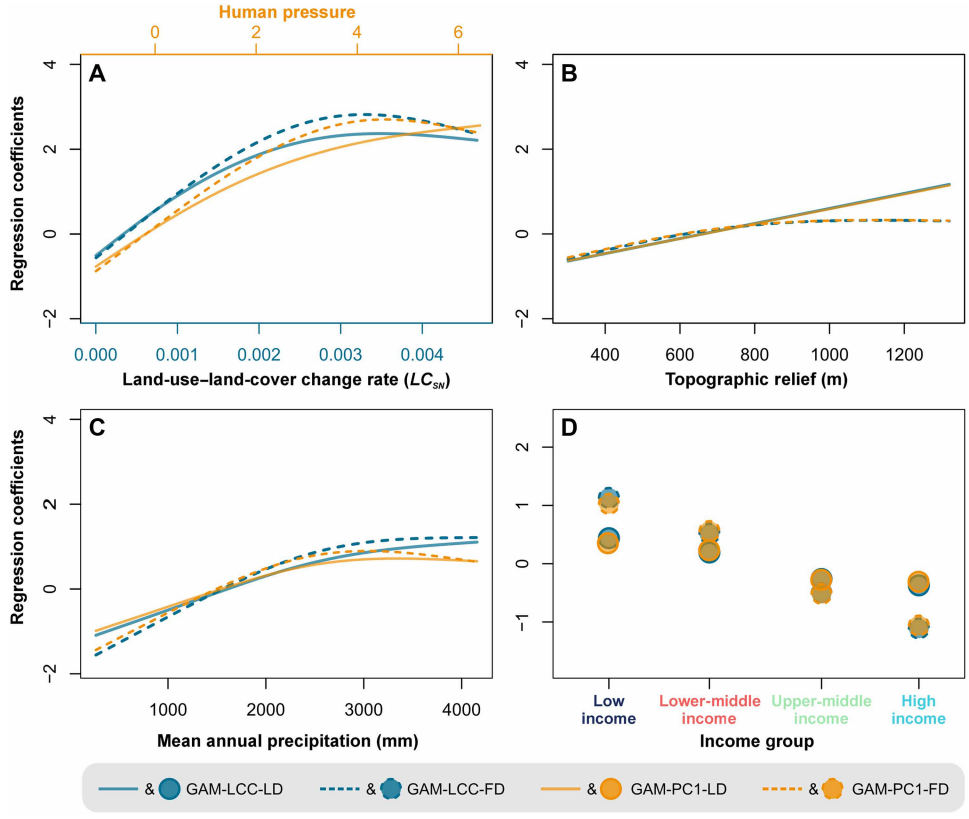

Fig. 4. Summary of the log-Gaussian GAMs, including four models (GAM-LCC and GAM–first principal component for *LD* and *FD*). Blue curves indicate GAM-LCC, and orange curves indicate GAM–first principal component (PC1), with solid lines representing the density of fatal landslides (*LD*) models and dashed lines representing the density of landslide fatalities (*FD*) models. Subplots show (**A**) LULCC rate (LC_{SN}) and human pressure (PC1), (**B**) topographic relief, (**C**) mean annual precipitation, and (**D**) income group. Results for each model are presented in separate figures in the Supplementary Materials: GAM-LCC-LD (fig. S17), GAM-LCC-FD (fig. S18), GAM-PC1-LD (fig. S19), and GAM-PC1-FD (fig. S20), along with 95% confidence intervals.

that LULCC and population growth are more pronounced in low- and lower-middle–income countries, leading to increased landslide occurrences and associated fatalities (*20*, *34*). Our analyses do not reveal a direct causal relationship between population growth, landslide counts, and respective fatalities. Hence, we propose that LULCC is an indirect major influence of the rising fatal landslide counts and their fatalities' densities.

Economic constraints limit the implementation of essential protection measures—often the primary key to immediate lifesaving—as well as adequate land-use–land-cover planning (*35*, *36*) and other disaster mitigation strategies (*37*), such as the implementation of landslide monitoring infrastructure. On the contrary, high-income countries can undertake effective disaster prevention and mitigation planning (*38*) to alleviate the potential impacts of land-use–land-cover on landslide risks. However, changes in land cover leave low- and lower-middle–income countries more exposed and vulnerable to the impacts of landslides. In addition, land-use–land-cover can act as a potential precondition or trigger for landslides and associated fatalities.

Interpretation

LULCC, as a potential landslide influence, is more prominent when national wealth is considered (Fig. 3, B, D, and F). Lower-income countries have a higher density of landslides and fatalities (Fig. 4D). In the same income category, rising LULCC rates are associated with an increase in the density of fatal landslides (*LD*) and the density of landslide fatalities (*FD*). For example, Rwanda's LULCC rate (LC_{SN}) is 10 times higher than Kenya's, corresponding to a threefold higher density of fatal landslides (*LD*) and a sevenfold higher density of landslide fatalities (*FD*) in the low-income category (table S5). However, this relation comes with considerable deviations.

Topographic relief and mean annual precipitation may additionally influence the interaction between LULCC rate (LC_{SN}), fatal landslides, and fatalities (Fig. 5). Hence, we made some comparisons considering these similarities to better understand the relationship. For example, in the lower-middle income category, Sri Lanka, Ecuador, and Guatemala have similar topographic relief and rainfall conditions. While Ecuador and Guatemala have comparable values in all three categories, Sri Lanka has a six times higher density of fatal landslides (*LD*) and about two times higher density of landslide fatalities (*FD*) on average. The only considerable difference that could impact this difference is the fivefold higher LULCC rate (LC_{SN}) in Sri Lanka than in others. Similarly, Haiti and India exhibit comparable topographic relief and rainfall features in the low-income category. Haiti, with an LULCC rate (LC_{SN}) about 150 times higher, has a density of landslide fatalities (*FD*) about fourfold times that of India (Fig. 5B).

Here, we fundamentally targeted the research question: Why are landslide fatalities higher in some countries despite wealth differences? We argue that countries with a lower LULCC rate (LC_{SN}) have a lower

Downloaded from https://www.science.org on April 08, 2026

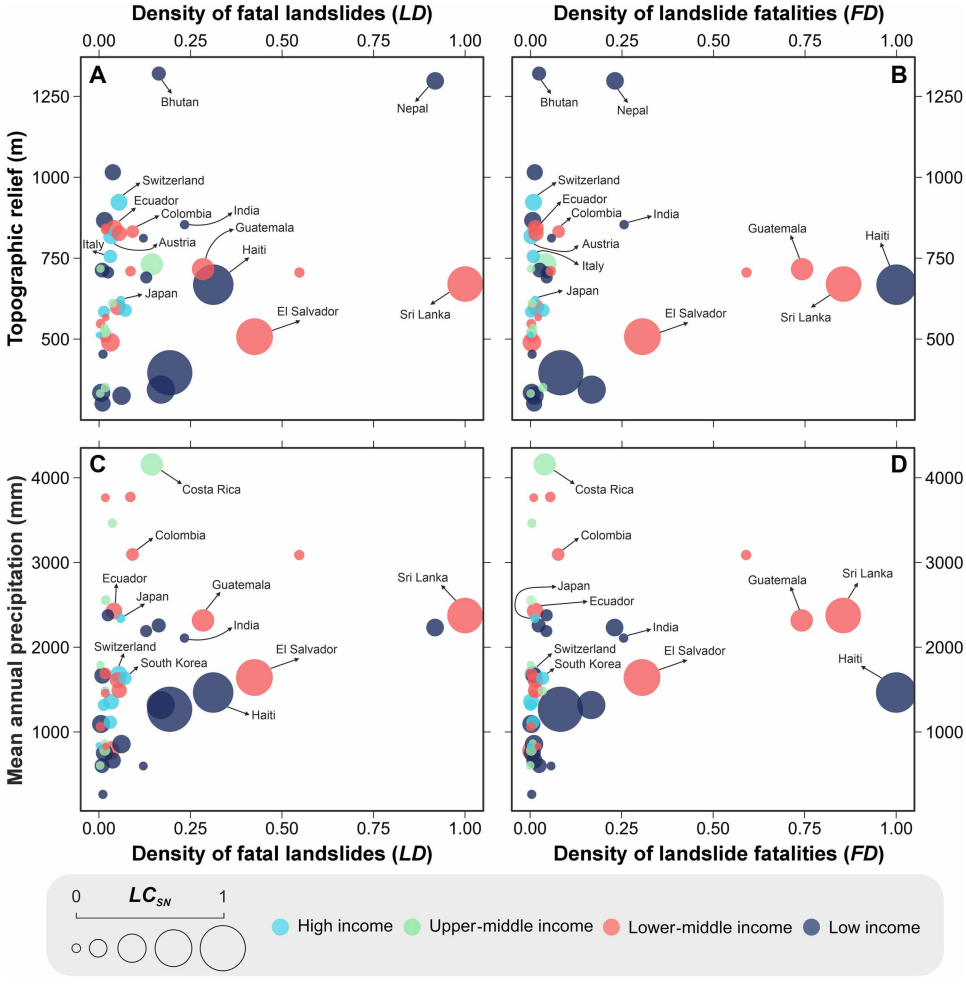

Fig. 5. The comparative density analysis of landslides and fatalities with topographic relief, precipitation, and LULCC rate (LC_{SN}) across income groups. Subplots (**A**) and (**B**) show the relationship between topographic relief and the density of fatal landslides (*LD*) and the density of landslide fatalities (*FD*), while subplots (**C**) and (**D**) illustrate the relationship between mean annual precipitation and *LD* and *FD*. Bubble size indicates LULCC rate (LC_{SN}), and colors represent income levels.

density of fatal landslides (*LD*) and a low density of landslide fatalities (*FD*) (Fig. 3). Although this may hold in general with several supporting examples on the country scale (Fig. 5), we also observed some outliers. For instance, Rwanda's LULCC rate (LC_{SN}) is three times higher, in contrast, the density of landslide fatalities (*FD*) is half of Uganda (table S5). Landslide hazards and human interactions are multifaceted and cannot be entirely explained by a single parameter. There may be secondary controls that need to be considered on different scales. We evaluated these potential secondary aspects in the subsection of limitations below.

LULCC-related indicators may provide information about a country's overall systemic vulnerability to natural hazards beyond landslides (e.g., (*39*). For example, between 1960 and 2019, Myanmar's urban area expanded by 150% (fig. S5), while its population increased by more than 1000% (fig. S7). The LULCC score (LC_S) is about 30% (overall mean: ≈26%; minimum: ≈2% in Canada and Malaysia; maximum: ≈96% in Tanzania; see tables S1 and S2). As a result, Myanmar shows a high fatality rate—29 fatalities per landslide. This systemic vulnerability was also reflected during the 2025 Mandalay Earthquake [moment magnitude (M_W): 7.7], which killed more than 3000 people and injured more than 4500. Having almost the same scores as Myanmar, Türkiye (LC_S: 32%; see table S1) has recently experienced a major earthquake, and we see similar results in fatalities (*40*). Hence, LULCC rate (LC_{SN}) may indicate a relationship between fatality and natural hazards beyond national wealth–based classification.

Exposure effect

Aside from all models, we included the exposure parameter as a controlling factor in the GAM-EXP (including exposure, LULCC rate, topographic relief, precipitation, and income) model to assess its effect (fig. S16). The model outputs show positive and substantial effects on the density of fatal landslides (*LD*) (fig. S23) and the density of landslide fatalities (*FD*) (fig. S24) and offer a higher fit than the GAM-LCC (including LULCC rate, topographic relief, precipitation, and income) and GAM-PC1 (including PC1, topographic relief, precipitation, and income) models in terms of performance metrics (table S6).

QQ plots show a distribution close to a straight line, and histograms are also close to normality (fig. S25). This convergence of model

Downloaded from https://www.science.org on April 08, 2026

residuals to a normal distribution supports the model's fit. However, we should exercise caution in interpreting these results. Because the study only considered landslides that resulted in death, all events included in the analysis already involved actual exposure. Therefore, this may lead to the exposure variable appearing artificially strong in the model. That is, an increase in both the density of fatal landslides (*LD*) and the density of landslide fatalities (*FD*) in areas with high exposure values is an expected outcome. This may indicate a cyclical dependency arising from the definition of the dataset rather than causality. This situation shows that the exposure factor may have limited interpretative power within this data framework. In upcoming studies using more comprehensive datasets that include nonfatal landslides, the actual impact of the exposure factor can be assessed more accurately. For this reason, the GAM-EXP model has been excluded from the primary model comparisons of the study and is only considered in the discussion section to explain potential bias.

Conceptual limitations

The level of disaster risk research in low-income countries is much less explored than in high-income nations despite higher fatality counts, increased exposure, and a high level of vulnerability (*41*, *42*). This contrast in the research community hinders the implementation of effective disaster prevention and mitigation strategies in low-income countries (*43*). In addition, socioeconomic constraints and weak governance limit, in some of these nations, the ability to adopt disaster reduction strategies, such as conservation and land-use–land-cover management measures (*44*). Directing research and funding to lesser-studied, high-risk regions can help fill knowledge gaps and strengthen the capacity of communities in these countries to cope with increasing hazard risk (*45*).

A notable example is Nepal (LC_S: 44.7% and LC_{SN}: 0.08; see tables S2), which may be classified as a low-income country with high landslide counts. Our analyses show that the fatalities are in the range of high-income nations (Fig. 5B). We suggest that, in this example, the international research efforts of the past decades dedicated to understanding landslide risk have paid off (*46*, *47*), especially when combined with local landslide hazard awareness (e.g., societal knowledge controls disaster risks) (*48*) and the high relative priority of landslide risk reduction within the spectrum of national hazards.

As stated in the interpretation subsection, we do not consider social controls other than wealth and LULCC metrics in this study. For example, in our comparison of Sri Lanka with Guatemala and Ecuador, one could argue that Sri Lanka faces different priorities due to more urgent societal challenges. However, the same could be said for Guatemala when considering other societal challenges. These can only marginally be captured by LULCC-related metrics that we have introduced. Therefore, we refrain from commenting on broader societal priorities directly, as they are beyond the scope of this study. Nevertheless, our interpretation should be viewed with the understanding that each country must be evaluated individually and that targeted policies should reflect their specific needs and societal contexts.

Data limitations

Policy decisions prioritizing economic growth over environmental sustainability often result in inadequate disaster preparedness and a greater risk of disasters (*45*). Because our study focuses solely on fatal landslides and aims to provide insights into the direct and indirect causes behind landslide fatalities in mountainous areas per income level, it excludes consideration of potentially nonfatal but economically damaging events. When the accuracy of landslide locations in data is improved with a more comprehensive range of landslide impacts, future research should assess the link between LULCC, landslides, and their economic consequences. These considerations, supported by our current analyses, would help evaluate the tangible and nontangible impact of unplanned land-use–land-cover management strategies from a landslide risk perspective (*49*).

The landslides have location uncertainties inherent in data derived from global databases. The location accuracy in the Global Fatal Landslide Database (GFLD) is based on administrative units such as villages or states (*1*). To bypass this limitation, we aggregated our analyses over mountainous areas that may extend across several of these units, their parts, or several countries (see Materials and Methods). This approach provided a more reliable framework to better understand the spatial overlap between fatal landslides and LULCC metrics we introduced.

Our analysis uses topographic relief and mean annual precipitation as primary indicators, which represent a methodological simplification of the complex geomorphic and climatic triggers of landslides. While fine-scale hillslope angles and extreme precipitation indices are more direct proxies for hillslope-scale instability, the inherent spatial uncertainty in global fatal landslide records and our country scale assessments (*1*) renders the use of high-resolution variables prone to substantial spatial noise. In this global-scale context, topographic relief serves as a robust descriptor of the broader mountainous environment, which inherently has steep gradients, showing a near-perfect correlation with hillslope angles at *r*: 0.99 in the K1 mountains (fig. S15). Similarly, mean annual precipitation provides a stable hydroclimatic signal that correlates strongly with maximum monthly precipitation (*r*: 0.87), making it a reliable descriptor for long-term conditions in global country comparisons. Nevertheless, we acknowledge that these macroscale variables may not capture the influence of local extremes or specific geological strength variations.

Using global-scale datasets within specific spatial boundaries of the K1 mountains can produce results that diverge from local observations. For instance, our finding of substantial forest loss in the mountainous areas of Rwanda (≈23%) contrasts with local-scale studies (*23*), which reported relatively stable forest cover since the 1950s. This discrepancy likely arises from the inherent characteristics and resolution of the global land-cover dataset used in our study (*24*), as well as our methodological focus on calculating LULCCs exclusively within the boundaries of the K1 mountains (*26*). These variations underscore the inherent limitations of the global products—which ensure cross-border consistency—with site-specific divergence that may provide higher resolution information potentially with different geographic scopes and classification definitions.

Beyond the spatial and resolution-related factors, the inherent reporting and linguistic biases within global databases also warrant consideration. Because the databases are primarily compiled from English-language media sources, such as the GFLD that we used, they are prone to underreporting in regions where English is not the primary language (*50*). This linguistic bias is particularly evident in the contrast between neighboring countries with different official languages and levels of international media attention. For example, our results for the Democratic Republic of Congo (DRC) and Rwanda may reflect differences in media coverage rather than physical landslide activity alone. While Rwanda receives substantial international attention, events in the DRC or Burundi—where French and other

Downloaded from https://www.science.org on April 08, 2026

local languages predominate—may be underreported unless they occur in areas of high geopolitical interest (e.g., conflict zones or mineral-rich regions) (*23*). These disparities in reporting frequency can lead to questionable values in the density of fatal landslides (*LD*) and the density of landslide fatalities (*FD*). The exclusion of countries such as Burundi from the analysis, despite its topographical similarities to Rwanda, further highlights the impact of these reporting thresholds. Therefore, it is important to interpret our findings cautiously, as they reflect the reported extent of landslide fatalities, not a complete global inventory.

Another substantial consideration should be the temporal scope of our land-use–land-cover analysis (1960 to 2019), which reflects our methodological choice to capture long-term anthropogenic pressures. This choice may lead to inconsistencies when compared to studies focusing on shorter, more recent intervals. While short-term landslide responses to LULCCs have been documented in specific regions [e.g., (*22*)], the impacts of such transformations can persist over extended periods. For example, increased landslide activity following deforestation may continue for 20 to 35 years (*51*) or even up to a century due to long-term alterations in geomorphic thresholds (*21*). Furthermore, it is well established that urbanization has a long-term effect on landslide susceptibility (*52*), as landslide occurrences may persist for several decades after land abandonment and subsequent vegetation recovery (*53*). In this context, we choose to use the (HIstoric Land Dynamics Assessment+) HILDA+ dataset (*24*), the longest interval that we are aware of, to account for these effects and to enable a comprehensive long-term assessment of land-use–land-cover dynamics in mountainous terrain. Consistent with this focus on general conditions rather than specific triggers, as our objective is not to find a link between the incidence of fatal landslides and the individual rainfall events, we concentrated on the mean annual precipitation as a proxy for the usual circumstances.

In many mountainous areas, forests help prevent landslides by providing slope stability (*22*, *54*). Hence, we categorized them as nonchange events and discounted them in our land-use–land-cover metrics (LC_S and LC_{SN}). While this assumption generally holds on a global scale, it may introduce biases in specific cases and local applications. For example, forest-type land-use–land-cover may become a surcharge load if shallow roots do not reach the rupture surface of underlying deep-seated landslides, such as those triggered by the 2016 Kumamoto Earthquake (*Mw*: 7.1) (*55*). Trees may also help transfer the wind force to the soil, leading to slope deformations (*56*).

Policy suggestion

Wealthier nations may experience fewer deaths from disasters (e.g., earthquakes, floods, hurricanes, extreme temperatures, and landslides), as they often already have the required resources and protection infrastructure (*38*). In contrast, countries with lower-income levels often lack the resources and infrastructure to mitigate and respond to such hazards effectively (*57*), making them more vulnerable to their impacts. This aspect is purely wealth driven. However, our analyses also revealed that the landslide fatalities are largely driven by land-use–land-cover transitions when income classes are considered. Hence, in low-income countries, effective land-use–land-cover management is critical to overcoming the adverse effects of population pressure and landslide fatalities and is likely to be the case for all disaster fatalities in general. Policies focusing on urban planning and rural development can help monitor land conversion in fragile mountain areas. If effective land-use–land-cover management solutions are implemented, then we may reduce fatal landslide counts and their fatalities.

MATERIALS AND METHODS

Extent

We focused exclusively on mountainous areas worldwide, where all analyzed variables were spatially masked using the K1 layer, including LULCC from 1960 to 2019. We examined the relationship between the rate of LULCC (hereafter referred to as *LC*) and fatal landslides at the country level by income class to shed light on the role of economic income level—high, upper-middle, lower-middle, and low income. However, the income classifications (wealth) of countries categorized by the World Bank change over time due to economic conditions (*58*). We identified the predominant income class using a frequency-based method to create a consistent income classification representing relative living standards that have changed over time. This income classification for all countries is reported in the source data file.

We use the income class based on per capita gross national income, according to the Atlas method (*59*). Moreover, we considered the median value (5.5) to ensure comparability across countries and only included countries with six or more fatal landslide events. This approach resulted in 46 countries grouped by wealth, allowing a more reliable comparison across countries: 7 high-income, 8 upper-middle–income, 15 lower-middle–income, and 16 low-income countries.

Landslide data

We obtained landslide records from the GFLD (2004 to 2017) (*1*). The database records fatal landslides triggered by nonseismic factors such as precipitation and human activities. The GFLD compiles landslide records from news reports, scientific studies, and government reports, providing information about location and associated accuracy, occurrence date, type, cause, and number of deaths.

We used landslides triggered by natural factors (i.e., precipitation and snow melt) and anthropogenic factors (i.e., construction, mining activities, hill cutting, and other human activities) corresponding to mountainous areas in the database. We aggregated landslide and fatality information using a repeated procedure for the mountain area of each country. We also calculated the density of fatal landslides (*LD*) and the density of landslide fatalities (*FD*) by dividing the number of landslides and deaths by the mountainous area of that country. This calculation led to a normalized measure of how concentrated landslides and fatalities are in different mountainous areas.

Global mountain data

We used the K1 layer, a previously published (*26*) comprehensive dataset describing mountainous areas on a global scale (Fig. 1A). The K1 layer classifies 24% of the Earth's land area as mountainous using a combination of elevation, hillslope angle, and relative relief at a 1-km resolution worldwide. All areas above 2500 m are considered mountainous regardless of relative relief, while areas below 2500 m are assigned as mountainous if their elevation and relative relief exceed 300 m. It also provides data appropriate for calculating forested areas in mountains and other land-use–land-cover (*60*).

We split the mountainous areas by country borders to explore land-use changes among countries with different income levels. We analyzed the *LC* specifically within these mountainous zones for countries with six or more fatal landslide events at the country level based on

Downloaded from https://www.science.org on April 08, 2026

income. Our analyses were performed over the mountainous areas of each country with a mean planimetric extent of 365,483 km^2 and a variation of 784,341 km^2 measured in one standard deviation (SD).

Land-use–land-cover data and change rate calculations

To explore the LULCC, we used HILDA+, a global land-use–land-cover dataset at a 1-km spatial resolution between 1960 and 2019 (*24*). HILDA+ is based on a data-driven reconstruction approach and combines many open data sources, such as high-resolution remote sensing and long-term land-use–land-cover reconstructions. This database includes six land-use–land-cover types: urban, cropland, pasture, forest, grass and shrubland, and sparse/no vegetation areas. We calculated each land-use–land-cover transition to capture differences in country-specific patterns and rates of change across these categories for the 59-year period from 1960 to 2019. In addition, to visualize the change between land-use–land-cover types, we created Sankey diagrams in RStudio using the "networkD3" package (*61*) to visualize the persistence of land-use–land-cover over the specified time interval and transitions between land-use–land-cover classes.

We followed four main steps to calculate the *LC*. In the first step, we derived absolute areas in urban, cropland, pasture, forest, grass and shrubland, and sparse/no vegetation regions from the HILDA database for the years 1960 and 2019, respectively. We then generated a transition matrix $T(t)$ representing the change between the six land-use–land-cover types from 1960 to 2019. In this matrix, each cell $T_{ij}(t)$ represents the area moving from land-use–land-cover type i to land-use–land-cover type j in year t. In the second step, we used this transition matrix to obtain the total areas of change for each land-use–land-cover type between 1960 and 2019. We calculated the total transition areas between each land-use–land-cover type using Eq. 1

$$LC_T = \sum_{i=1}^{6} \sum_{j=1}^{6} T_{ij}(t) \tag{1}$$

where LC_T represents the total *LC*. Repeating this procedure for 46 countries provided the basis for analyzing the dynamics of *LC* at the country level by income class.

As the third step, we assigned a score corresponding to the dynamics of *LC* in each of the 46 countries to obtain a total *LC* rate. For this computation, we classified transitions between all land-use–land-cover categories into change (e.g., conversion to another type) and nonchange events (e.g., unchanged areas and conversions to forest) and converted area transitions into percentages. Because, in many mountainous areas, forests help prevent landslides by providing slope stability (*22*, *54*), we categorized them as nonchange events. We calculated the rate of change, which is the sum of the percentages of conversion from one land-use–land-cover type to another, using Eq. 2

$$LC_S = \sum_{\substack{i=1 \\ i \neq j \\ j \neq \text{forest}}}^{6} \sum_{j=1}^{6} P_{ij}(t) \tag{2}$$

where LC_S represents the total *LC* rate, $P_{ij}(t)$ represents the percentage of area transitioned from land-use–land-cover type i to land-use–land-cover type j, $i \neq j$ excludes unchanged areas, and j ≠ forest excludes transitions to forests. A higher LC_S value indicates that the land-use–land-cover in a specific country's mountainous areas is considerably changing, while a lower LC_S value means minimal change and less intervention (tables S1 and S2).

Last, we normalized the total rate of *LC* by each country's mountainous area to calculate the intensity of its change by area and obtain a comparable measure. For each country and its associated *LC*, we apply the following Eq. 3

$$LC_{SN} = \frac{LC_S}{A_{mountain}} \tag{3}$$

where LC_{SN} represents the normalized LC_S and $A_{mountain}$ represents the total mountainous area of the country (tables S1 and S2).

Population data

To estimate population pressure in potentially mountainous areas, we used population grids at a 30–arc sec (≈1 km) spatial resolution (GHS-POP R2023A, a product of Global Human Settlement). GHS-POP R2023A provides the distribution of the human population expressed as the number of people per cell (*25*). Because of the lack of historical population data going back to 1960 (the year from which land-use–land-cover data became available), we used data from 1975 onward, and using population data from the GHS-POP product, we obtained the total number of individuals for each country's mountainous area for 1975 and 2020 (fig. S7). We then calculated the population change rate (*PC*) as follows in Eqs. 4 and 5

$$PC = \left(\frac{Mountain_{pop2020}}{Mountain_{pop1975}} - 1 \right) \tag{4}$$

$$PC_N = \frac{PC}{A_{mountain}} \tag{5}$$

where $Mountain_{pop2020}$ is the total population in 2020 and $Mountain_{pop1975}$ is the total population in 1975. We also normalized this by each country's mountainous area ($A_{mountain}$) to obtain a comparable measure (PC_N), and this procedure was repeated for each country. Details per country are in tables S4 and S5.

Exposure and population density

Exposure and population density were estimated using GHS-POP data (2005, 2010, and 2015) for years when fatal landslides were recorded. For each country, the mean population for mountainous areas was calculated using the K1 layer data during the landslide recording period.

To estimate the magnitude of exposure, we quantify physical exposure (*E*) to fatal landslides by adopting the framework used in the United Nations Development Programme Disaster Risk Index. Physical exposure is defined as the product of hazard frequency and the population residing in the affected area (*62*, *63*). We calculated the physical exposure for each mountainous areas using the following formula

$$E = L_i \, x \, \overline{P} \tag{6}$$

where L_i represents the hazard frequency, defined as the total number of fatal landslides recorded within the country's mountainous areas, and $\overline{P}$ is the mean population in these areas during the observation period. This multiplicative logic, intersecting event frequency with

Downloaded from https://www.science.org on April 08, 2026

population, aligns with established practices for characterizing human exposure to landslide hazards (e.g., *64*). Population density (*PD*) was calculated by dividing the same mean population by the total mountainous area ($A_{mountain}$) of the country

$$PD = \frac{\overline{P}}{A_{mountain}} \quad (7)$$

This approach ensures consistency by relying on a temporally consistent population dataset and a spatially consistent definition of mountainous areas.

Topographic relief and precipitation analysis

Topographic variables, including both hillslope angles and relief, were systematically derived from the Multi-Error-Removed Improved-Terrain–Digital Elevation Model at a 1-km pixel resolution (*65*). To estimate local topographic relief, we calculated the difference in elevation between the highest and lowest elevations within a 2.5-km radius. Preliminary correlation analysis revealed a very high collinearity between hillslope angles and relief (*r*: 0.99) (fig. S15). Because of this high collinearity and our focus on mountainous areas, topographic relief was prioritized over hillslope angle (i.e., steepness). We choose topographic relief, as it captures the local relative elevation differences better than steepness alone, providing a more comprehensive descriptor of the mountainous area.

For precipitation analysis across mountain regions, we used the CHELSA v2.1 climate dataset (*66*), which offers a 30–arc sec (≈1 km) spatial resolution. We extracted the long-term mean annual precipitation layer (BIO12) over the past 30 years (1981 to 2010) to account for the spatial precipitation gradient. Our aim is not to link fatal landslide occurrences to the respective rainfall events. We focused on mean annual precipitation as a proxy for average conditions. We also evaluated the maximum monthly precipitation (BIO13), which exhibited a high correlation (*r*: 0.87) with BIO12 (fig. S15). On the basis of this strong relationship, BIO12 was used as a robust proxy for reflecting spatial precipitation patterns.

Generalized additive model

The GAM is a flexible statistical framework that can estimate both linear and nonlinear relationships between explanatory variables and the response variable (*67*). GAMs are particularly useful for estimating landslide susceptibility using the Bernoulli distribution (*68*, *69*), landslide intensity using the Poisson distribution (*70*), and landslide area using the Gaussian distribution. To model continuous outcomes such as landslide area or landslide intensity, it is necessary to account for the heavy-tailed distribution of such variables. For this purpose, continuous landslide metrics are typically subjected to log transformation, making log-Gaussian GAM a suitable option for statistical modeling (*71*, *72*).

In our study, both the density of fatal landslides (*LD*) and the density of landslide fatalities (*FD*), which are continuous response variables, exhibit skewed distributions. Hence, we applied a logarithmic transformation to both variables and assumed a log-Gaussian distribution within the GAM framework (fig. S14). This choice helped in approximating complex nonlinear relationships among the different explanatory variables, e.g., anthropogenic, climatic, and topographic.

We considered a set of controlling factors: LULCC rate (LC_{SN}), population change rate (PC_N), population density (*PD*), exposure (*E*), topographic relief, mean annual precipitation, and income group. We show the statistical structure of our model using a Conceptual Directed Acyclic Graph. These diagrams represent the assumed causal relationships between the main explanatory variables and the response variables, the density of landslides and fatalities (fig. S16). As our primary model, we developed GAM-LCC, in which LULCC rate (LC_{SN}) was used directly to represent anthropogenic pressure

$$\log(\mu_i) = \beta_0 + f_1(LC_{SNi}) + f_2(\text{Relief}_i) + f_3(\text{Precip}_i) + f_4(\text{Income}_i) \quad (8)$$

where μ_i is the expected value of the log-transformed density of fatal landslides (*LD*) or the density of landslide fatalities (*FD*) in mountain unit *i*; β_0 is the intercept term; f_1 (LC_{SN}) models the direct effect of *LC*; f_2 (Relief_i) captures the effect of topographic relief; f_3 (Precip_i) represents the influence of long-term mean annual precipitation; and f_4 (Income_i) accounts for the effect of countries' income group, treated as an ordinal socioeconomic variable. To evaluate the robustness of our results and test the sensitivity of the anthropogenic representation, we developed an alternative model—referred to as GAM-PC1—based on PCA. Because of strong multicollinearity among LC_{SN}, PC_N, and *PD* (fig. S15)—all of which reflect overlapping anthropogenic processes—we extracted the PC1, which explained about 90% of the variance, and interpreted it as a composite "human pressure" indicator (table S3). The GAM-PC1 model was specified as follows

$$\log(\mu_i) = \beta_0 + f_1(\text{PC1}_i) + f_2(\text{Relief}_i) + f_3(\text{Precip}_i) + f_4(\text{Income}_i) \quad (9)$$

where all terms are as defined above, with f_1 ($PC1_i$) representing the smooth effect of the composite anthropogenic factor derived from LC_{SN}, PC_N, and *PD*.

In addition to GAM-LCC and GAM-PC1, we fitted a third model—GAM-EXP—which explicitly included exposure as a predictor. However, this model—GAM-EXP—was treated independently due to interpretational limitations inherent to the dataset. Because our analysis only targeted fatal landslides, all recorded events include exposure to the hazard. Thus, including exposure in the model additionally creates a reinforcing cycle. As a result, its inclusion risks circular reasoning, whereby higher exposure trivially leads to more observed fatalities or reported events. This model was excluded from our primary comparisons and is discussed separately in Discussion

$$\log(\mu_i) = \beta_0 + f_1(E_i) + f_2(\text{Relief}_i) + f_3(\text{Relief}_i) + f_4 + f_5(\text{Income}_i) \quad (10)$$

where f_1 (E_i) models the effect of exposure and all other terms retain their previous definitions. For all models, the log-Gaussian GAM fitted is based on the "mgcv" R package (*67*). We used series of metrics, including root mean square error (RMSE), mean absolute error (MAE), Pearson correlation coefficient (*R*), Nash-Sutcliffe efficiency (NSE), and AIC, to evaluate models performances. While RMSE and MAE reflect the average prediction error, *R* and NSE indicate how well the model captures the observed variation, and AIC is used to compare model fit. In addition to these numerical indicators, we visually inspected model fit and residual structure using three diagnostic plots: observed versus fitted values, QQ plots, and histograms of residuals (*67*).

Downloaded from https://www.science.org on April 08, 2026

Supplementary Materials

The PDF file includes:

Supplementary Text
Figs. S1 to S25
Tables S1 to S6
Legend for data file S1

Other Supplementary Material for this manuscript includes the following:

Data file S1

REFERENCES

1. M. J. Froude, D. N. Petley, Global fatal landslide occurrence from 2004 to 2016. *Nat. Hazards Earth Syst. Sci.* **18**, 2161–2181 (2018).
2. M. Klose, P. Maurischat, B. Damm, Landslide impacts in Germany: A historical and socioeconomic perspective. *Landslides* **13**, 183–199 (2016).
3. D. N. Petley, Fatal landslides in 2024 (The Landslide Blog, 2025); https://eos.org/thelandslideblog/fatal-landslides-in-2024.
4. M. Guns, V. Vanacker, Shifts in landslide frequency-area distribution after forest conversion in the tropical Andes. *Anthropocene* **6**, 75–85 (2014).
5. J. C. Maki Mateso, C. L. Bielders, E. Monsieurs, A. Depicker, B. Smets, T. Tambala, L. Bagalwa Mateso, O. Dewitte, Characteristics and causes of natural and human-induced landslides in a tropical mountainous region: The rift flank west of Lake Kivu (Democratic Republic of the Congo). *Nat. Hazards Earth Syst. Sci.* **23**, 643–666 (2023).
6. L. Pisano, V. Zumpano, C. M. Malek, M. P. Rosskopf, Variations in the susceptibility to landslides, as a consequence of land cover changes: A look to the past, and another towards the future. *Sci. Total Environ.* **601-602**, 1147–1159 (2017).
7. S. Fidan, H. Tanyaş, A. Akbaş, L. Lombardo, D. N. Petley, T. Görüm, Understanding fatal landslides at global scales: A summary of topographic, climatic, and anthropogenic perspectives. *Nat. Hazards* **120**, 6437–6455 (2024).
8. I. B. Bennett, P. R. Bierman, A century of urban landslides: The legacy and consequences of altering riverbank landscapes. *Q. J. Eng. Geol. Hydrogeol.* **57**, qjegh2023-032 (2024).
9. P. R. Elsen, W. B. Monahan, A. M. Merenlender, Topography and human pressure in mountain ranges alter expected species responses to climate change. *Nat. Commun.* **11**, 1974 (2020).
10. J. M. Thornton, M. A. Snethlage, R. Sayre, D. R. Urbach, D. Viviroli, D. Ehrlich, V. Muccione, P. Wester, G. Insarov, C. Adler, Human populations in the world's mountains: Spatio-temporal patterns and potential controls. *PLOS ONE* **17**, e0271466 (2022).
11. D. Ehrlich, M. Melchiorri, C. Capitani, Population trends and urbanisation in mountain ranges of the world. *Land* **10**, 255 (2021).
12. U. Ozturk, E. Bozzolan, E. A. Holcombe, R. Shukla, F. Pianosi, T. Wagener, How climate change and unplanned urban sprawl bring more landslides. *Nature* **608**, 262–265 (2022).
13. D. R. Montgomery, K. M. Schmidt, H. M. Greenberg, W. E. Dietrich, Forest clearing and regional landsliding. *Geology* **28**, 311–314 (2000).
14. K. Ullah, Y. Wang, P. Li, Z. Fang, M. Rahaman, S. Ullah, M. M. Hamed, Spatiotemporal dynamics of landslide susceptibility under future climate change and land use scenarios. *Environ. Res. Lett.* **19**, 124016 (2024).
15. V. Vanacker, M. Vanderschaeghe, G. Govers, E. Willems, J. Poesen, J. Deckers, B. De Bievre, Linking hydrological, infinite slope stability and land-use change models through GIS for assessing the impact of deforestation on slope stability in high Andean watersheds. *Geomorphology* **52**, 299–315 (2003).
16. H. Tanyaş, T. Görüm, D. Kirschbaum, L. Lombardo, Could road constructions be more hazardous than an earthquake in terms of mass movement? *Nat. Hazards* **112**, 639–663 (2022).
17. D. N. Petley, Æ. G. J. Hearn, Æ. A. Hart, N. J. Rosser, Æ. S. A. Dunning, Æ. K. Oven, W. A. Mitchell, Trends in landslide occurrence in Nepal. *Nat. Hazards* **43**, 23–44 (2007).
18. N. Wood, J. Jones, Vations in road exposure and traffic volumes in the United States in areas susceptible to landslides. *Int. J. Disaster Risk Reduct.* **124**, 105567 (2025).
19. X. Wang, Y. Wang, Q. Lin, X. Yang, Assessing global landslide casualty risk under moderate climate change based on multiple GCM projections. *Int. J. Disaster Risk Sci.* **14**, 751–767 (2023).
20. A. Gatto, F. Martellozzo, S. Clo', L. Ciulla, S. Segoni, The downward spiral entangling soil sealing and hydrogeological disasters. *Environ. Res. Lett.* **19**, 084023 (2024).
21. T. Glade, Landslide occurrence as a response to land use change: A review of evidence from New Zealand. *Catena* **51**, 297–314 (2003).
22. N. Grima, D. Edwards, F. Edwards, D. Petley, B. Fisher, Landslides in the Andes: Forests can provide cost-effective landslide regulation services. *Sci. Total Environ.* **745**, 141128 (2020).
23. A. Depicker, L. Jacobs, N. Mboga, B. Smets, A. Van Rompaey, M. Lennert, E. Wolff, F. Kervyn, C. Michellier, O. Dewitte, G. Govers, Historical dynamics of landslide risk from population and forest-cover changes in the Kivu Rift. *Nat. Sustain.* **4**, 965–974 (2021).
24. K. Winkler, R. Fuchs, M. Rounsevell, M. Herold, Global land use changes are four times greater than previously estimated. *Nat. Commun.* **12**, 2501 (2021).
25. M. Schiavina, S. Freire, A. Carioli, K. MacManus, GHS-POP R2023A - GHS population grid multitemporal (1975-2030), European Commission, Joint Research Centre (2023); doi:10.2905/2FF68A52-5B5B-4A22-8F40-C41DA8332CFE.
26. V. Kapos, J. Rhind, M. Edwards, M. F. Price, C. Ravilious, "Developing a map of the world's mountain forests," in *Forests in Sustainable Mountain Development*, M. Price N. Butt, Eds. (CABI Publishing, 2000), pp. 4–9.
27. H. Garcia-Delgado, D. N. Petley, M. A. Bermúdez, S. A. Sepúlveda, Fatal landslides in Colombia (from historical times to 2020) and their socio-economic impacts. *Landslides* **19**, 1689–1716 (2022).
28. E. Aristizábal, O. Sánchez, Spatial and temporal patterns and the socioeconomic impacts of landslides in the tropical and mountainous Colombian Andes. *Disasters* **44**, 596–618 (2020).
29. S. L. Gariano, F. Guzzetti, Landslides in a changing climate. *Earth Sci. Rev.* **162**, 227–252 (2016).
30. A. Felsberg, J. Poesen, M. Bechtold, M. Vanmaercke, G. J. M. De Lannoy, Estimating global landslide susceptibility and its uncertainty through ensemble modelling. *Nat. Hazards Earth Syst. Sci.* **22**, 3063–3082 (2022).
31. T. Stanley, D. B. Kirschbaum, A heuristic approach to global landslide susceptibility mapping. *Nat. Hazards* **87**, 145–164 (2017).
32. S. Fankhauser, T. K. J. McDermott, Understanding the adaptation deficit: Why are poor countries more vulnerable to climate events than rich countries? *Glob. Environ. Change* **27**, 9–18 (2014).
33. J. V. Ferrer, C. B. Moroz, S. Yüksel, O. Dewitte, K. Lebek, N. Marwan, J. Kurths, O. Korup, Exposure to large landslides in cities outpaces urban growth. *Geophys. Res. Lett.* **52**, e2025GL115170 (2025).
34. E. C. Johnston, F. V. Davenport, L. Wang, J. K. Caers, S. Muthukrishnan, M. Burke, N. S. Diffenbaugh, Quantifying the effect of precipitation on landslide hazard in urbanized and non-urbanized areas. *Geophys. Res. Lett.* **48**, e2021GL094038 (2021).
35. A. Hailu, S. Mammo, M. Kidane, Dynamics of land use, land cover change trend and its drivers in Jimma Geneti District, Western Ethiopia. *Land Use Policy* **99**, 105011 (2020).
36. M. M. Maja, S. F. Ayano, The impact of population growth on natural resources and farmers' capacity to adapt to climate change in low-income countries. *Earth Syst. Environ.* **5**, 271–283 (2021).
37. I. Schumacher, E. Strobl, Economic development and losses due to natural disasters: The role of hazard exposure. *Ecol. Econ.* **72**, 97–105 (2011).
38. M. E. Kahn, D. Costa, S. Gerking, E. Glaeser, A. Levinson, J. Shapiro, J. Shimshack, C. Timmins, The death toll from natural disasters: The Role of income, geography, and institution. *Rev. Econ. Stat.* **87**, 271–284 (2005).
39. O. Renn, M. Laubichler, K. Lucas, W. Kröger, J. Schanze, R. W. Scholz, P. J. Schweizer, Systemic risks from different perspectives. *Risk Anal.* **42**, 1902–1920 (2022).
40. T. Görüm, H. Tanyas, F. Karabacak, A. Yılmaz, S. Girgin, K. E. Allstadt, M. L. Süzen, P. Burgi, Preliminary documentation of coseismic ground failure triggered by the February 6, 2023 Türkiye earthquake sequence. *Eng. Geol.* **327**, 107315 (2023).
41. L. Stein, S. K. Mukkavilli, B. M. Pfitzmann, P. W. J. Staar, U. Ozturk, C. Berrospi, T. Brunschwiler, T. Wagener, Wealth over Woe: Global biases in hydro-hazard research. *Earth's Future* **12**, e2024EF004590 (2024).
42. J. V. Ferrer, G. S. Mohor, O. Dewitte, T. Pánek, C. R. Carmona, A. L. Handwerger, M. Hürlimann, L. Köhler, K. Teshebaeva, A. H. Thieken, C. Y. Tsou, A. U. Vinueza, V. Demurtas, Y. Zhang, C. Zhao, N. Marwan, J. Kurths, O. Korup, Human settlement pressure drives slow - moving landslide exposure. *Earth's Future* **12**, e2024EF004830 (2024).
43. I. Alcántara-Ayala, Geomorphology, natural hazards, vulnerability and prevention of natural disasters in developing countries. *Geomorphology* **47**, 107–124 (2002).
44. J. Maes, C. Parra, K. Mertens, B. Bwambale, L. Jacobs, J. Poesen, O. Dewitte, L. Vranken, A. De Hontheim, C. Kabaseke, M. Kervyn, Questioning network governance for disaster risk management: Lessons learnt from landslide risk management in Uganda. *Environ. Sci. Policy* **85**, 163–171 (2018).
45. I. Alcántara-ayala, Landslides in a changing world. *Landslides* **22**, 2851–2865 (2025).
46. A. Dahal, L. Lombardo, Towards physics-informed neural networks for landslide prediction. *Eng. Geol.* **344**, 107852 (2024).
47. J. N. Jones, S. J. Boulton, M. Stokes, G. L. Bennett, M. R. Z. Whitworth, 30-year record of Himalaya mass-wasting reveals landscape perturbations by extreme events. *Nat. Commun.* **12**, 6701 (2021).
48. P. Bubeck, U. Ozturk, E. Aristizabal, A. H. Thieken, T. Wagener, Mortality reduction despite changing climate extremes requires better understanding of human behavioral response to warnings. *Environ. Res. Lett.* **20**, 101004 (2025).
49. P. Sibomana, M. Vanmaercke, A. Depicker, B. Tychon, O. Dewitte, Effects of agricultural terraces on landslide occurrence: Insights from a tropical mountainous region (Rwanda, Africa). *Catena* **253**, 108898 (2025).
50. D. Gómez, E. F. García, E. Aristizábal, Spatial and temporal landslide distributions using global and open landslide databases. *Nat. Hazards* **117**, 25–55 (2023).
51. R. H. Guthrie, The effects of logging on frequency and distribution of landslides in three watersheds on Vancouver Island, British Columbia. *Geomorphology* **43**, 273–292 (2002).

Downloaded from https://www.science.org on April 08, 2026

52. T. Rohan, E. Shelef, B. Mirus, T. Coleman, Prolonged influence of urbanization on landslide susceptibility. *Landslides* **20**, 1433–1447 (2023).
53. S. Beguerı, Changes in land cover and shallow landslide activity: A case study in the Spanish Pyrenees. *Geomorphology* **74**, 196–206 (2006).
54. P. Brang, W. Schönenberger, M. Frehner, R. Schwitter, J.-J. Thormann, B. Wasser, Management of protection forests in the European Alps: An overview. *Forest Snow Landsc. Res.* **80**, 23–44 (2006).
55. S. Von Specht, U. Ozturk, G. Veh, F. Cotton, O. Korup, Effects of finite source rupture on landslide triggering: The 2016 Mw 7.1 Kumamoto earthquake. *Solid Earth* **10**, 463–486 (2019).
56. E. Parra, C. H. Mohr, O. Korup, Predicting patagonian landslides: Roles of forest cover and wind speed. *Geophys. Res. Lett.* **48**, e2021GL095224 (2021).
57. S. Lindersson, E. Raffetti, M. Rusca, L. Brandimarte, J. Mård, G. Di Baldassarre, The wider the gap between rich and poor the higher the flood mortality. *Nat. Sustain.* **6**, 995–1005 (2023).
58. World Bank, World Bank country and lending groups (2024); https://datahelpdesk.worldbank.org/knowledgebase/articles/906519-world-bank-country-and-lending-groups.
59. World Bank, World Bank open data (2023); https://data.worldbank.org/indicator/NY.GNP.PCAP.CD?view=chart [accessed 11 January 2023].
60. R. Sayre, C. Frye, D. Karagulle, J. Krauer, S. Breyer, P. Aniello, D. J. Wright, D. Payne, C. Adler, H. Warner, D. P. Vansistine, J. Cress, A new high-resolution map of world mountains and an online tool for visualizing and comparing characterizations of global mountain distributions. *Mt. Res. Dev.* **38**, 240–249 (2018).
61. J. J. Allaire, C. Gandrud, K. Russell, C. J. Yetman, networkD3: D3 JavaScript network graphs from R (CRAN, 2017); https://cran.r-project.org/web/packages/networkD3/networkD3.pdf.
62. P. Peduzzi, H. Dao, C. Herold, F. Mouton, Assessing global exposure and vulnerability towards natural hazards: The disaster risk index. *Nat. Hazards Earth Syst.* **9**, 1149–1159 (2009).
63. United Nations Development Programme, "A global report: Reducing disaster risk, a challenge for development" (New York, 2004).
64. R. Emberson, D. Kirschbaum, T. Stanley, New global characterisation of landslide exposure. *Nat. Hazards Earth Syst. Sci.* **20**, 3413–3424 (2020).
65. D. Yamazaki, D. Ikeshima, R. Tawatari, T. Yamaguchi, F. O'Loughlin, J. C. Neal, C. C. Sampson, S. Kanae, P. D. Bates, A high-accuracy map of global terrain elevations. *Geophys. Res. Lett.* **44**, 5844–5853 (2017).
66. D. N. Karger, O. Conrad, J. Böhner, T. Kawohl, H. Kreft, R. W. Soria-Auza, N. E. Zimmermann, H. P. Linder, M. Kessler, Climatologies at high resolution for the Earth's land surface areas. *Sci. Data* **4**, 170122 (2017).
67. S. N. Wood, *Generalized Additive Models: An Introduction with R* (Chapman and Hall/CRC, ed. 2, 2017).
68. S. Steger, A. Brenning, R. Bell, H. Petschko, T. Glade, Exploring discrepancies between quantitative validation results and the geomorphic plausibility of statistical landslide susceptibility maps. *Geomorphology* **262**, 8–23 (2016).
69. G. Titti, C. van Westen, L. Borgatti, A. Pasuto, L. Lombardo, When enough is really enough? On the minimum number of landslides to build reliable susceptibility models. *Geosci.* **11**, 469 (2021).
70. L. Lombardo, H. Bakka, H. Tanyas, C. van Westen, P. M. Mai, R. Huser, Geostatistical modeling to capture seismic-shaking patterns from earthquake-induced landslides. *Case Rep. Med.* **124**, 1958–1980 (2019).
71. M. Di Napoli, H. Tanyas, D. Castro-Camilo, D. Calcaterra, A. Cevasco, D. Di Martire, G. Pepe, P. Brandolini, L. Lombardo, On the estimation of landslide intensity, hazard and density via data-driven models. *Nat. Hazards* **119**, 1513–1530 (2023).
72. L. Lombardo, H. Tanyas, R. Huser, F. Guzzetti, D. Castro-Camilo, Landslide size matters: A new data-driven, spatial prototype. *Eng. Geol.* **293**, 106288 (2021).

Acknowledgments: This study was supported by the Istanbul Technical University Scientific Research Projects Coordination Unit under grant number MDK-2021-43288. We thank the support of the Istanbul Technical University Scientific Research Projects Coordination Unit. T.G. acknowledges support from the Scientific and Technological Research Council of Türkiye (TUBITAK) through 2247-A National Outstanding Researchers Program grant number 1199B472343092. U.O. is funded by the European Union (ERC, UrbanSlide, grant 101160656; doi: 10.3030/101160656). Views and opinions expressed are, however, those of the author(s) only and do not necessarily reflect those of the European Union or the European Research Council. Neither the European Union nor the granting authority can be held responsible for them. **Funding:** This work was supported by the NATO Science for Peace and Security Program (SPS grant number G6190). **Author contributions:** Conceptualization: S.F., T.G., A.A., B.E., and U.O. Data curation: S.F. and A.A. Formal analysis: S.F., T.G., and A.A. Funding acquisition: T.G. Investigation: S.F., T.G., A.A., and B.E. Methodology: S.F., T.G., A.A., and B.E. Project administration: S.F. Resources: S.F. and A.A. Software: S.F. Supervision: S.F., T.G., A.A., B.E., and U.O. Validation: S.F., A.A., and B.E. Visualization: S.F., T.G., and U.O. Writing—original draft: S.F., T.G., A.A., B.E., and U.O. Writing—review and editing: S.F., T.G., A.A., B.E., and U.O. **Competing interests:** The authors declare that they have no competing interests. **Data, code, and materials availability:** The Global Fatal Landslide Database (GFLD) is available freely at the landslide blog (https://blogs.agu.org/landslideblog/2019/06/18/global-fatal-landslide-database-1/). The K1 mountain range boundary can be accessed at https://doi.org/10.1659/MRD-JOURNAL-D-17-00107.1. The Global Human Settlement Layer (GHSL) is accessible at https://human-settlement.emergency.copernicus.eu/download.php?ds=pop. HILDA+ (HIstoric Land Dynamics Assessment+) is provided at https://doi.pangaea.de/10.1594/PANGAEA.921846?format=html#download. The analysis codes used in this study are openly accessible at https://doi.org/10.5281/zenodo.16793081. All data and code needed to evaluate and reproduce the results in the paper are present in the paper and/or the Supplementary Materials. This study did not generate new materials.

Submitted 13 September 2025
Accepted 11 March 2026
Published 8 April 2026
10.1126/sciadv.aec2739

Downloaded from https://www.science.org on April 08, 2026

ScienceAdvances

Wealth and land-cover change govern landslide fatalities on world's mountains

Seçkin Fidan, Tolga Görüm, Abdullah Akba#, Bikem Ekberzade, and Ugur Ozturk

Sci. Adv. **12** (15), eaec2739. DOI: 10.1126/sciadv.aec2739

View the article online
https://www.science.org/doi/10.1126/sciadv.aec2739
Permissions
https://www.science.org/help/reprints-and-permissions

Downloaded from https://www.science.org on April 08, 2026

Use of this article is subject to the Terms of service

Science Advances (ISSN 2375-2548) is published by the American Association for the Advancement of Science. 1200 New York Avenue NW, Washington, DC 20005. The title *Science Advances* is a registered trademark of AAAS.

Copyright © 2026 The Authors, some rights reserved; exclusive licensee American Association for the Advancement of Science. No claim to original U.S. Government Works. Distributed under a Creative Commons Attribution NonCommercial License 4.0 (CC BY-NC).